

Preoperative Three-Dimensional Model Creation of Magnetic Resonance Brain Images as a Tool to Assist Neurosurgical Planning

B.S. Spottiswoode^{a, c, g} D.J. van den Heever^d Y. Chang^b S. Engelhardt^h
S. Du Plessis^e F. Nicolls^b H.B. Hartzenberg^f A. Gretscheff^f

^aMRC/UCT Medical Imaging Research Unit, Department of Human Biology, and ^bDepartment of Electrical Engineering, University of Cape Town, Cape Town, ^cDivision of Radiology, ^dBiomedical Engineering Research Group, Department of Mechanical and Mechatronic Engineering, ^eDepartment of Psychiatry, and ^fDivision of Neurosurgery, Stellenbosch University, Stellenbosch, South Africa; ^gCardiovascular MR R&D, Siemens Healthcare, Chicago, Ill., USA; ^hComputational Visualistics, University of Koblenz-Landau, Koblenz, Germany

Key Words

Stereolithography · Three-dimensional printing · Neurosurgery · Magnetic resonance imaging · Functional magnetic resonance imaging · Rapid prototyping

Abstract

Background: Neurosurgeons regularly plan their surgery using magnetic resonance imaging (MRI) images, which may show a clear distinction between the area to be resected and the surrounding healthy brain tissue depending on the nature of the pathology. However, this distinction is often unclear with the naked eye during the surgical intervention, and it may be difficult to infer depth and an accurate volumetric interpretation from a series of MRI image slices. **Objectives:** In this work, MRI data are used to create affordable patient-specific 3-dimensional (3D) scale models of the brain which clearly indicate the location and extent of a tumour relative to brain surface features and important adjacent structures. **Methods:** This is achieved using custom software and rapid prototyping. In addition, functionally eloquent areas identified using functional MRI are integrated into the 3D models. **Results:** Preliminary in vivo results are presented for

2 patients. The accuracy of the technique was estimated both theoretically and by printing a geometrical phantom, with mean dimensional errors of less than 0.5 mm observed. **Conclusions:** This may provide a practical and cost-effective tool which can be used for training, and during neurosurgical planning and intervention. Copyright © 2013 S. Karger AG, Basel

Introduction

In this work, magnetic resonance imaging (MRI) data are processed to create patient-specific 3-dimensional (3D) scale models of the brain using rapid and affordable technology called medical rapid prototyping (RP). These models may be useful clinically as they clearly indicate the location and extent of a tumour relative to brain surface features and important adjacent structures.

Neurosurgeons regularly plan their surgery using a series of MRI images taken at a variety of image planes. MRI provides excellent image contrast between soft tissue types, and a number of 3D image classification and segmentation techniques have been developed to iden-

tify and isolate specific anatomical structures [1]. MRI images are capable of showing a clear distinction between a tumour and the surrounding brain tissue in certain pathologies and are essential in preoperative planning. The role of neurosurgical planning in resection of brain tumours is to define the safest possible approach with minimal permanent damage to normal brain tissue [2, 3]. Functional MRI (fMRI), which indirectly reflects brain activity by measuring the regional haemodynamic response to a specific task, may further be incorporated in surgical planning procedures [4, 5]. The fMRI results can influence the entry point and trajectory of the surgical intervention to avoid damaging eloquent cortical areas. The most commonly used fMRI tasks for neurosurgical planning are tactile, motor, language and visual [4].

Although modern software is capable of improving one's 3D interpretation by rendering object surfaces and allowing free navigation through 3D image data, these images are typically scaled and are ultimately being viewed on a 2D screen where a correct depth perception is difficult to achieve. Medical RP has been used in a wide range of biomedical applications, most notably in modelling and reconstructing bone features [6–14]. Medical RP may be defined as the manufacture of dimensionally accurate physical models of human anatomy derived from medical image data using a variety of 3D printing or RP technologies [15]. We propose creating physical, 3D scale models of the brain with the tumour in situ, which the surgeon can use to plan the surgery using the gyral/sulcal surface markings. 3D printing technology can be used to make case-specific scale models that are cost-effective and quick to produce. Such neurosurgical models can provide a practical alternative for operating theatres which are unable to afford the integrated stereotactic planning equipment. Furthermore, the models are hands-on, intuitive, and can be used to rehearse the procedures. Although MRI images have been used with RP technologies to create models of the brain [7], we have found no reference to cases where 3D models with brain surface features have been extracted from MRI data and used for surgical planning. Other MRI techniques, such as fMRI, diffusion tensor imaging [16] or MR angiography, can further be used to provide additional information on the 3D model to aid in neurosurgical planning. Previous preliminary work has been done using RP to define MRI-derived fibre tracts [17] and vessel anatomy [18], but to our knowledge no previous work has been done combining fMRI and RP technologies.

We have created a software interface for neurosurgeons to navigate through the MRI data, identify the region to be resected, integrate fMRI activation, plan the surgical trajectory, and create the files necessary for the printing of a hands-on 3D scale model of the brain. This paper describes the development of this software, quantifies the accuracy of the 3D models, and presents preliminary case studies from 2 patients.

Methods

Case Studies

Two patients with a lesion in the proximity of the motor cortex were scanned using a 3-tesla MRI scanner (MAGNETOM Allegra, Siemens AG, Germany). Ethical approval and informed consent were obtained in accordance with requirements of the Health Research Ethics Committee at Stellenbosch University, South Africa. High-resolution T1-weighted 3D magnetization-prepared rapid gradient echo (MPRAGE) MRI images [19], which provide excellent contrast between grey and white matter, were acquired with the following imaging parameters: TR = 2,300 ms, TE = 3.93 ms, TI = 1,100 ms, flip angle = 9°, spatial resolution = $1 \times 1 \times 1 \text{ mm}^3$, matrix size = 256×256 , slices = 160, FOV = 256 mm, bandwidth = 651 Hz/pixel, scan time = 9:50. fMRI data were acquired using an echo planar imaging sequence with TR = 2,000 ms, TE = 30 ms, slices = 34, spatial resolution = $3.8 \times 3.8 \times 3.5 \text{ mm}^3$, matrix size = 64×64 , FOV = 240 mm, measurements/volumes = 121, scan time = 4:06. Both hand and foot motor tasks were performed to map motor function, and each task involved 30-second interleaved periods of rest and activity.

Multilevel preprocessing was performed using FSL (FMRIB, Oxford, UK), which is a comprehensive library of analysis tools for medical data [20]. The resulting images were fed into a custom software tool developed for rapidly and accurately converting 3D MRI images into scale 3D physical models. FSL was used to derive fMRI activation maps, coregister/fuse the low-resolution fMRI images to the MPRAGE image, and extract the grey matter from the MPRAGE image. fMRI statistical maps were extracted at a threshold of $p < 0.05$ (corrected for multiple comparisons), and the first echo planar imaging volume was coregistered to the MPRAGE image. The MPRAGE image was then classified into grey matter, white matter and cerebrospinal fluid using a non-binary partial volume map. The white matter and cerebrospinal fluid volumes were then discarded for several reasons: only the pial surface is required to identify landmarks; the fMRI regions are limited to the grey matter, and the amount of material used in the RP process should be minimized to save printing costs.

Custom software was developed using the MeVisLab v.2.2 (MeVis Medical Solutions AG, Bremen, Germany) framework which provides modules for medical image processing as well as visualization and interaction methods [21]. A dedicated graphical user interface allows the user to select the region of interest, mark the lesion, identify the relevant fMRI regions and set a surgical trajectory. A splitting plane can then be defined to separate the volume for better viewing of the lesion, surgical trajectory and fMRI regions. Isosurfaces are constructed using a neighbouring

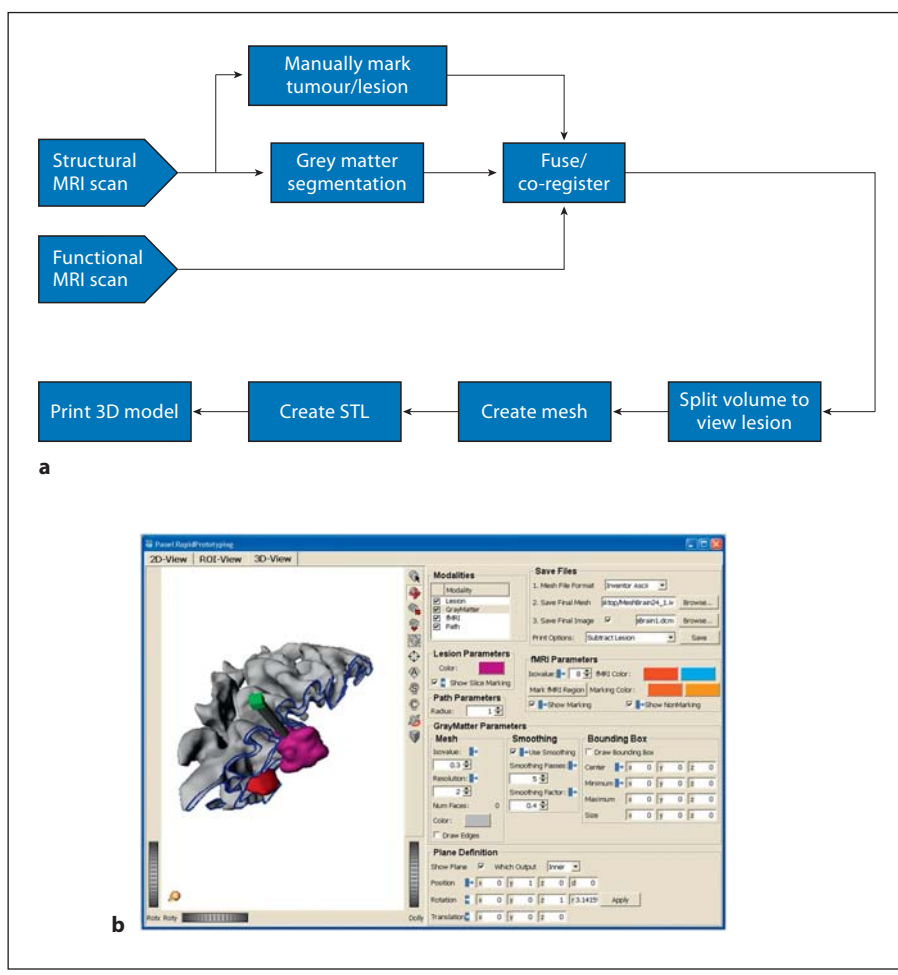


Fig. 1. a Data processing overview. **b** The user interface developed in MeVisLab.

cells algorithm and Laplacian surface smoothing is incorporated during meshing. Finally, the files necessary for 3D printing are created. Figure 1 outlines the steps involved and shows the software interface.

Printing of the model was performed on a Z510 Spectrum (3D Systems, Rock Hill, S.C., USA) system which is capable of printing at a high spatial resolution (in-plane = $0.042 \times 0.047 \text{ mm}^2$; layer thickness = 0.089 mm). For the first patient, the entire cerebrum and cerebellum were printed as a proof-of-concept. In the case of the second patient, a smaller brain region was printed to minimize costs, the lesion and fMRI regions were manually painted for clarity, and the model was compared to the actual brain surface during surgery. Printing was performed using an acrylic polymer and the printing time amounted to roughly 12 and 2 h for the first and second patients, respectively, and costs of roughly USD 300 and 30, respectively.

Error Estimation

The accuracy of the 3D models was estimated both theoretically and using simulated phantom experiments with physical measurements and repeat MRI scans. The potential sources of error along the scanning, processing and printing pipeline include

(1) errors inherent in the MRI scanning procedure, (2) errors introduced during the meshing and smoothing, (3) errors introduced during the printing and (4) coregistration errors which may be present for the fMRI data. The coregistration errors are not central to this work and are thus not investigated further.

The errors inherent in the MRI scan are largely due to gradient field (B1) distortions, principal magnetic field (B0) inhomogeneities, and subject-specific susceptibility artefacts. The true gradient field was estimated using spherical harmonic expansion [22]. Here, the B1 image distortions were approximated using a table of coefficients of the spherical harmonics provided by the vendor. The B0 and object-induced distortions were estimated using the method described by Jezard and Balaban [23], where phase maps from multiple echoes are combined to yield the pixel shift in the phase encode direction. For this, two echoes from the MPRAGE acquisition ($TE1/TE2 = 1.5/6.6 \text{ ms}$) were used.

A phantom validation was performed to assess the accuracy of the model and quantify any differences between the real object and the printed object. A geometric MRI phantom with overall dimensions of $100 \times 100 \times 100 \text{ mm}^3$ and a range of scaled surface features, shown in figure 2, was designed using MATLAB (The Mathworks, Natick, Mass., USA). The sum of the printing

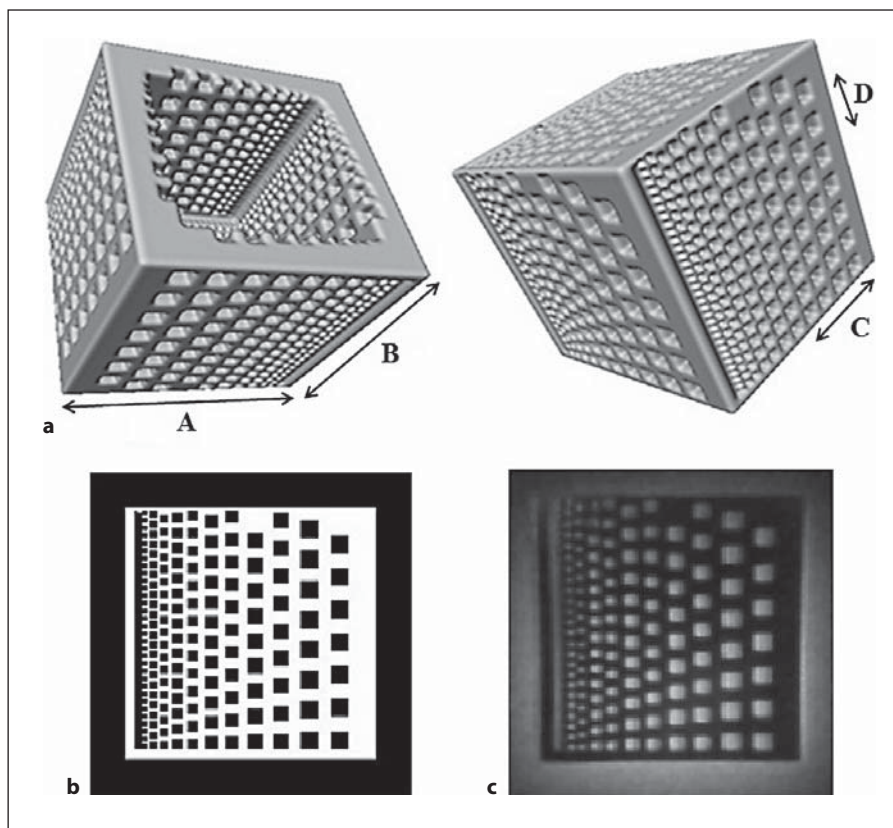


Fig. 2. Validation phantom ($100 \times 100 \times 100 \text{ mm}^3$) created in MATLAB. **a** Rendered 3D views. **b** Simulated model. **c** Scanned phantom (immersed in water). The position of the slice in **b** and **c** is near the periphery of the phantom where the largest field inhomogeneities are expected. Both partial volume effects and B0 distortions are evident in **c**.

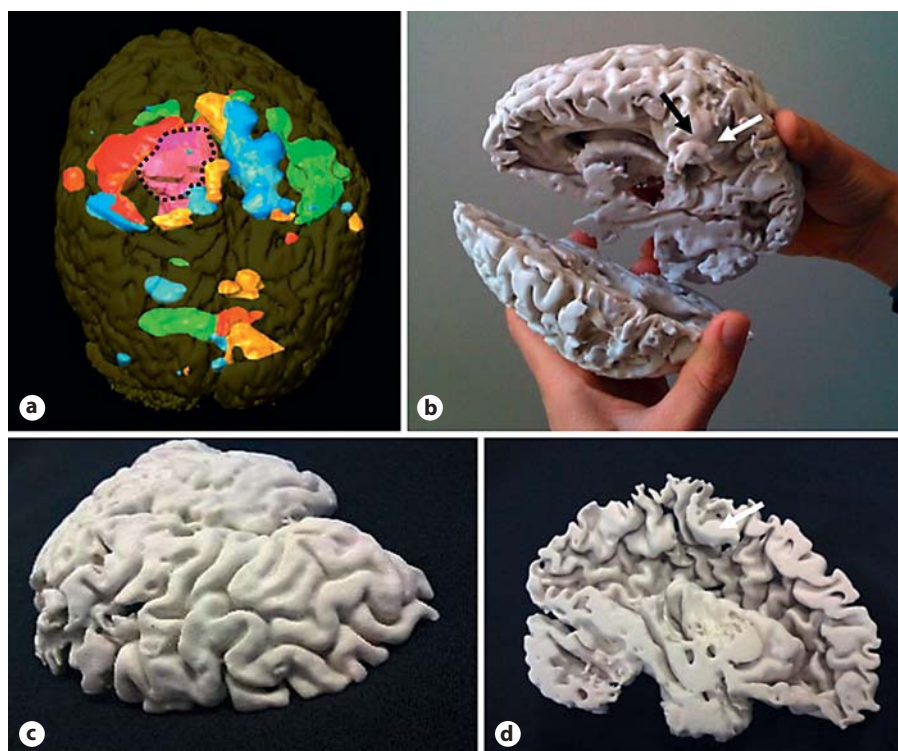


Fig. 3. Example of printing the whole brain using RP. **a** Reference rendered image created using iPlan Cranial 3.0 (Brainlab, AG, Germany). The tumour is indicated using dotted lines. Regions of activation identified using fMRI are also shown; these include right hand (red); right foot (orange); left hand (green); left foot (blue; for colours, see online version). **b** Corresponding patient-specific 3D rapid prototype model, with the white arrow indicating the tumour and the black arrow indicating the right hand motor area as identified using fMRI. Note that the splitting plane is defined as a sagittal slice in the left hemisphere that bisects the tumour. **c, d** Details of the gyral and sulcal grey matter features, respectively. The white arrow indicates the tumour.

error (defined by the vendor) and the meshing and smoothing error can be estimated by making manual measurements on the printed phantom. Manual measurements were made on the printed phantom using a Vernier calliper (accuracy of 0.02 mm). In total, 40 measurements were taken in all three spatial directions (XYZ) with a range of 2–100 mm. Several of these measurements can be seen in figure 2. Each feature on the model has a specific known dimension, and measuring over a combination of these features results in a collection of measurements with varying dimensions. The accumulated scanning, printing and meshing errors can be estimated by scanning the printed phantom and comparing this to the theoretical MATLAB model. This was achieved by immersing the phantom in water and scanning with the identical MPRAGE imaging parameters described above. Further measurements were made on the scanned phantom directly from the DICOM images. For each of the 40 measurements, a dimensional error (mm) was calculated as the absolute error between the theoretical MATLAB phantom model and the printed and scanned phantoms. Relative differences (%) were also calculated as the dimensional difference divided by the theoretical phantom model value $\times 100$. This method was used in previous studies [24, 25]. Comparisons between the measurements were made with the Student t test for paired samples. Differences were taken as statistically significant at $p < 0.05$.

Results

Figure 3 shows the whole-brain RP model from the first patient, where the splitting plane was defined as a sagittal slice bisecting the tumour. The fMRI volumes were attached to one side of the split model, giving a clear indication of the proximity to the tumour. The detailed grey matter surface features can be appreciated in figure 3c and d. Figure 4 shows the printed model for the second patient, where coloured paint was added to more clearly identify the lesion and fMRI activation. The depth and extent of the tumour are clearly evident, and the gyri/sulci provide structures for intuitive navigation when compared to the actual brain surface.

The maximum gradient field distortion was estimated to be 2–3 mm and the maximum B0 distortion in the readout direction was estimated to be 0.15 mm. The 3D printed phantom had a mean dimensional error of 0.5 mm (standard deviation 0.19 mm) and a mean relative error of 4.6% (standard deviation 6.7%) over the entire range of measurements. The MRI scanned phantom had a mean dimensional error of 0.4 mm (standard deviation 0.6 mm) and a mean relative error of 2.3% (standard deviation 4.1%). Differences between the theoretical and 3D printed phantom were not statistically significant ($p = 0.12$), but the differences between the theoretical and the MRI scanned phantom were significant ($p = 0.02$).

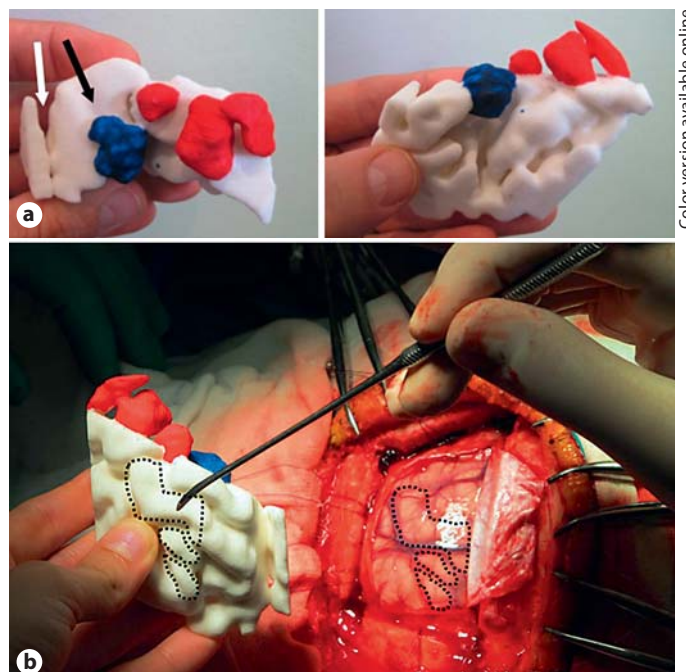


Fig. 4. **a** 3D printed model showing a lesion (to the left in blue) and fMRI regions (to the right in red; for colours, see online version) corresponding to right-hand activation. Left: Posterior view, right: inferior view. The white arrow shows the brain midline and the black arrow shows the planned surgical trajectory. **b** Corresponding gyral/sulcal features on the exposed brain are indicated using dotted lines.

Discussion

Several stereotactic solutions have been developed to plan and perform surgery guided by MRI images with reported localization accuracy of less than 1 mm [26]. However, these systems are expensive and the shifts in brain position occurring during the craniotomy may result in the unnecessary removal of viable tissue, with recorded shifts at the cortical surface of up to 24 mm [27]. Medical RP has been used in a wide range of biomedical applications, including surgical planning, training of doctors, disease diagnosis and in patient education [8, 10–17, 28–30]. RP enables quick and cost-effective fabrication of case-specific models that are dimensionally accurate. This presents huge potential in a range of applications in the medical field. In its simplest form, RP produces 3D models by building up the model layer by layer using a quick setting glue-like material. Research and development in the field have resulted in newer RP technologies with lower costs and shorter manufacturing

times than traditional stereolithography [25]. 3D printing can be used to print on various materials (including plastics, metals, wax, and rubber-like materials) and in different colours, and even allows the simultaneous printing of different materials and different colours. The technology has also been used to print using biomaterials and even human tissue [31–33]. Benefits to RP for surgery, as identified by Müller et al. [12] and Kalejs and von Segesser [28], are as follows: (1) a better understanding of anatomical relations for surgical planning, with resulting improved intra-operative accuracy in the localization of lesions; (2) improved tactile understanding of an anatomical object; (3) provides opportunities for the surgeon to rehearse the operation realistically; (4) improved communication between the surgeon and the patient; (5) more accurate fabrication of implants, and (6) permanent recordings for future requirements or reconstructions.

In this study, MRI data were used to create patient-specific 3D scale models of the brain to provide a practical and cost-effective tool which can be used during neurosurgical planning and intervention. Integrating fMRI data into the 3D models introduces additional information that can influence the entry point and trajectory of the surgical intervention in order to avoid damaging eloquent cortical areas. The gyri/sulci provide structures for intuitive navigation when compared to the actual brain surface. The models further give clear indications of the depth and extent of the tumours and their spatial relationship to eloquent cortical areas. From figure 4, it is evident that printing only a region of interest can result in difficulty with orientation. This can be overcome by viewing the rendered whole brain volume (with the printed region highlighted) on a computer screen or printout. Different MRI techniques can also provide detailed information about vessel anatomy, white matter fibre architecture, and functional brain activation. It is possible to add any of these features onto the RP model with appropriate colour coding for further refinements to the surgical planning. Furthermore, modern 3D printers allow for printing with multiple materials and even soft materials, which could be used to rehearse neurosurgical procedures.

Unusual or unexpected image appearances, referred to as artefacts, are associated with all medical imaging techniques [16]. MRI is prone to imaging errors caused by gradient field distortions, principal field inhomogeneities, and subject-specific susceptibility artefacts. It is also important to analyse parameters in the RP process to ensure accuracy. In the 3D printing system, parameters that

must be controlled to obtain a reliable model include the printing mechanism, the type and quality of the materials used, and the absorption properties of the material when in contact with the binder [25]. However, the limiting factor in model accuracy remains with the imaging technique. This is due to the relatively low resolution of typical 3D imaging techniques compared to the build resolution of most modern RP systems. In our case, the MRI has an imaging resolution of $1 \times 1 \times 1 \text{ mm}^3$, whereas the 3D printing system has a build resolution of $0.042 \times 0.047 \times 0.089 \text{ mm}^3$.

A geometric phantom model with a range of scaled surface features was designed and fabricated with a 3D printer, in order to assess the accuracy of the models. Comparing the printed model to the theoretical model gave an indication of the sum of the printing error and the meshing and smoothing error. The printed model was immersed in water and MRI scanned with the identical MPRAGE imaging parameters as for the 2 case studies. This provided a method to estimate the full combination of errors inherent in the process by comparing the scanned model to the theoretical model. The measured errors were considerably smaller than the estimated errors due to B0 and B1 distortions. The reason for this is likely because of the relatively small size of the printed phantom relative to the scanner field of view. Over the range of measurements (2–100 mm) in all spatial directions (XYZ) the 3D printed model showed a mean relative error of 4.6% (standard deviation 6.7%). This is slightly higher compared to the accuracy reported by Silva et al. [25], who showed a mean error of 2.67% when using 3D printing to make cranial prototypes. It is worth noting, however, that the smallest feature they measured was larger than 26 mm, compared to the smallest feature of 2 mm in this study. A 20% error on a 2-mm feature is still accurate to within 0.4 mm. When only taking into account measurements of 10 mm and greater, the mean relative error of the 3D printed model drops to 0.69% (standard deviation 1.23%).

The scanned phantom showed better results compared to the printed model with a mean relative error of 2.29% (standard deviation 4.1%). This could be due to small artefacts on the printed models which are incorporated in the calliper measurements but are not present on the scanned model. When only looking at measurements greater than 10 mm, the relative accuracy drops to 1.21% (standard deviation 1.63%), which is greater than the printed model, suggesting that these small artefacts only play a role on the small scale features.

The dimensional accuracy found in this study may be satisfactory for these scale models to provide a practical and intuitive tool to be used for training purposes and to assist with neurosurgical planning. With the price of 3D printing dropping as the technology becomes more common, this may provide a cost-effective alternative for operating theatres which are unable to afford the integrated stereotactic planning equipment. Furthermore, the models are hands-on, intuitive, and can be used to improve communication with the patient and to rehearse the surgical procedures. Future work will include more clearly defining the brain surface using an advanced cortical mapping technique such as Freesurfer [34], and validating the technique on a spectrum of patients using a stereotactic position sensor.

Conclusion

We have successfully produced rapid prototyped scale models of human grey matter. Through a phantom validation experiment, the models are shown to have acceptable accuracy, with a mean dimensional error of less than 0.5 mm. To our knowledge, this is the first time RP has been combined with fMRI. The technique may provide a practical and hands-on tool for training and surgical planning.

Acknowledgements

We thank Mr. John Coetzee from the University of Cape Town for his assistance with the 3-dimensional printing; Siemens Medical Solutions South Africa, and the staff at the Cape Universities Brain Imaging Centre.

References

- Rengier F, von Tengg-Kobligh H, Zechmann C, Kauczor HU, Giesel FL: Beyond the eye – medical applications of 3D rapid prototyping objects. *Eur Med Imaging Rev* 2008;1: 76–80.
- Tharin S, Golby A: Neurosurgical treatment planning; in Newton HB, Jolesz FA (eds): *Handbook of Neuro-Oncology Neuroimaging*. New York, Academic Press, 2008, pp 181–191.
- Kettenbach J, Wong T, Kacher D, Hata N, Schwartz RB, Black P McL, Kikinis R, Jolesz FA: Computer-based imaging and interventional MRI: applications for neurosurgery. *Comput Med Imaging Graph* 1999;23:245–258.
- Hirsch J, Ruge MI, Kim KHS, Correa DD, Victor JD, Relkin NR, Labar DR, Krol G, Bilsky MH, Souweidane MM, DeAngelis LM, Gutin PH: An integrated functional magnetic resonance imaging procedure for preoperative mapping of cortical areas associated with tactile, motor, language, and visual functions. *Neurosurgery* 2000;47:711–722.
- Geerts J, Martens M, Vandevenne JE, Gelin G, Grieten M, Weyns F, Stinissen P, Palmers Y, Wuyts J: Functional magnetic resonance imaging for preoperative localisation of eloquent brain areas relative to brain tumours: clinical implementation in a regional hospital. *JBR-BTR* 2007;90:258–263.
- Swann S: Integration of MRI and stereolithography to build medical models: a case study. *Rapid Prototyping J* 1996;2:41–46.
- Berry E, Brown JM, Connell M, Craven CM, Efford ND, Radjenovic A, Smith MAS: Preliminary experience with medical applications of rapid prototyping by selective laser sintering. *Med Eng Phys* 1997;19:90–96.
- Foroutan M, Fallahi B, Mottavalli S, Dujovny M: Stereolithography: application to neurosurgery. *Crit Rev Neurosurg* 1998;8: 203–208.
- McGurk M, Potamianos P, Amis AA, Goodger NM: Rapid prototyping techniques for anatomical modelling in medicine. *Ann R Coll Surg Engl* 1997;79:169–174.
- Kai CC, Meng CS, Ching LS, Hoe EK, Fah LK: Rapid prototyping assisted surgery planning. *Int J Adv Manuf Technol* 1998;14:624–630.
- Webb PA: A review of rapid prototyping (RP) techniques in the medical and biomedical sector. *J Med Eng Technol* 2000;24:149–153.
- Müller A, Krishnan KG, Uhl E, Mast G: The application of rapid prototyping technologies in cranial reconstruction and preoperative planning in neurosurgery. *J Craniofac Surg* 2003;14:899–914.
- Cunningham Jr LL, Madsen MJ, Peterson G: Stereolithographic modeling technology applied to tumor resection. *J Oral Maxillofac Surg* 2005;63:873–878.
- Waran V, Devaraj P, Hari Chandran T, Muthusamy KA, Rathinam AK, Balakrishnan YK, Tung TS, Raman R, Rahman ZAA: Three-dimensional anatomical accuracy of cranial models created by rapid prototyping techniques validated using a neuronavigation station. *J Clin Neurosci* 2012;19:574–577.
- Winder J, Bibb R: Medical rapid prototyping technologies: state of the art and current limitations for applications in oral and maxillofacial surgery. *J Oral Maxillofac Surg* 2005; 63:1006–1015.
- Yu CS, Li KC, Xuan Y, Ji XM, Qin W: Diffusion tensor tractography in patients with cerebral tumors: a helpful technique for neurosurgical planning and postoperative assessment. *Eur J Radiol* 2005;56:197–204.
- Acevedo D, Zhang S, Laidlaw DH, Bull CW: Color rapid prototyping for diffusion tensor MRI visualization. *Proc MICCAI, Saint-Malo, September 2004*, pp 1076–1078.
- Markl M, Schumacher R, Küffer J, Bley TA, Hennig J: Rapid vessel prototyping: vascular modeling using 3T magnetic resonance angiography and rapid prototyping technology. *MAGMA* 2005;18:288–292.
- Mugler JP III, Brookeman JR: Three-dimensional magnetization-prepared rapid gradient-echo imaging (3D MP RAGE). *Magn Reson Med* 1990;15:152–157.
- Smith SM, Jenkinson M, Woolrich MW, Beckmann CF, Behrens TEJ, Johansen-Berg H, Bannister PR, De Luca M, Drobnjak I, Flitney DE, et al: Advances in functional and structural MR image analysis and implementation as FSL. *Neuroimage* 2004;23:208–219.
- Hahn HK, Link F, Peitgen H: Concepts for rapid application prototyping in medical image analysis and visualization. *Proc Simulation Visualisierung, Ghent, March 2003*, pp 283–298.
- Janke A, Zhao H, Cowin GJ, Galloway GJ, Doddrell GM: Use of spherical harmonic deconvolution methods to compensate for nonlinear gradient effects on MRI images. *Magn Reson Med* 2004;52:115–122.
- Jezzard P, Balaban RS: Correction for geometric distortion in echo planar images from B0 field variations. *Magn Reson Med* 1995; 34:65–73.

- 24 Chang PS, Patrick TH, Patrick CW Jr, Miller MJ: The accuracy of stereolithography in planning craniofacial bone replacement. *J Craniofac Surg* 2003;14:164–170.
- 25 Silva DN, Gerhardt de Oliveira M, Meurer E, Meurer MI, Lopes da Silva JV, Santa-Barbara A: Dimensional error in selective laser sintering and 3D-printing of models for cranio-maxillary anatomy reconstruction. *J Craniomaxillofac Surg* 2008;36:443–449.
- 26 Fengqiang L, Jiadong Q, Yi L: Computer-assisted stereotactic neurosurgery with framework neurosurgery navigation. *Clin Neurol Neurosurg* 2008;110:696–700.
- 27 Hastreiter P, Rezk-Salama C, Soza G, Bauer M, Greiner G, Fahlbusch R, Ganslandt O, Nimsy C: Strategies for brain shift evaluation. *Med Image Anal* 2004;8:447–464.
- 28 Kalejs M, von Segesser LK: Rapid prototyping of compliant human aortic roots for assessment. *Interact Cardiovasc Thorac Surg* 2008;8:182–186.
- 29 Taft RM, Kondor S, Grant GT: Accuracy of rapid prototype models for head and neck reconstruction. *J Prosthet Dent* 2011;106:399–408.
- 30 Faber J, Berto PM, Quaresma M: Rapid prototyping as a tool for diagnosis and treatment planning for maxillary canine impaction. *Am J Orthod Dentofacial Orthop* 2006;129:583–589.
- 31 Mironov V, Boland T, Trusk T, Forgacs G, Markwald RR: Organ printing: computer-aided jet-based 3D tissue engineering. *Trends Biotechnol* 2003;21:157–161.
- 32 Mironov V, Visconti RP, Kasyanov V, Forgacs G, Drake CJ, Markwald RR: Organ printing: tissue spheroids as building blocks. *Biomaterials* 2009;30:2164–2174.
- 33 Mironov V, Kasyanov V, Markwald RR: Organ printing: from bioprinter to organ bio-fabrication line. *Curr Opin Biotechnol* 2011;22:667–673.
- 34 Fischl B, Salat DH, Busa E, Albert M, Dieterich M, Haselgrove C, van der Kouwe A, Killiany R, Kennedy D, Klaveness S, Montillo A, Makris N, Rosen B, Dale AM: Whole brain segmentation: automated labelling of neuroanatomical structures in the human brain. *Neuron* 2002;33:341–355.